Accurate and Practical Thruster Modeling for Underwater Vehicles

Jinhyun Kim, Wan Kyun Chung *

Robotics & Bio-Mechatronics Lab. Pohang Univ. of Sci. & Tech. (POSTECH), Pohang, 790-784, Korea (Republic of)

Abstract

The thruster is the crucial factor of an underwater vehicle system, because it is the lowest layer in the control loop of the system. In this paper, we propose an accurate and practical thrust modeling for underwater vehicles which considers the effects of ambient flow velocity and angle. In this model, the axial flow velocity of the thruster, which is non-measurable, is represented by ambient flow velocity and propeller shaft velocity. Hence, contrary to previous models, the proposed model is practical since it uses only measurable states. Next, the whole thrust map is divided into three states according to the state of ambient flow and propeller shaft velocity, and one of the borders of the states is defined as *Critical Advance Ratio (CAR)*. This classification explains the physical phenomenon of conventional experimental thrust maps. In addition, the effect of the incoming angle of ambient flow is analyzed, and *Critical Incoming Angle (CIA)* is also defined to describe the thrust force states. The proposed model is evaluated by comparing experimental data with numerical model simulation data, and it accurately covers overall flow conditions within ±2N force error. The comparison results show that the new model's matching performance is significantly better than conventional models'.

Key words: Thrusters, underwater vehicle, thrust modeling, advance ratio, incoming angle

* Corresponding author. Tel.: +82-54-279-2172; fax: +82-54-279-5899.
Email addresses: pluto@postech.ac.kr (Jinhyun Kim), wkchung@postech.ac.kr (Wan Kyun Chung).

1 Introduction

Thruster modeling and control are the core of underwater vehicle control and simulation, because it is the lowest control loop of the system; hence, the system would benefit from accurate and practical modeling of the thrusters. In unmanned underwater vehicles, thrusters are generally propellers driven by electrical motors. Therefore, thrust force is simultaneously affected by motor model, propeller map, and hydrodynamic effects, and besides, there are many other facts to consider (Manen and Ossanen, 1988), which make the modeling procedure difficult. To resolve the difficulties, many thruster models have been proposed.

In the classical analysis of thrust force under steady-state bollard pull conditions, a propeller's steady-state axial thrust (T) is modeled proportionally to the signed square of propeller shaft velocity (Ω), $T = c_1\Omega|\Omega|$ (Newman, 1977). Yoerger et al. (1990) presented a one-state model which also contains motor dynamics. To represent the four-quadrant dynamic response of thrusters, Healey et al. (1995) developed a two-state model with thin-foil propeller hydrodynamics using sinusoidal lift and drag functions. This model also contains the ambient flow velocity effect, but it was not dealt with thoroughly. In Whitcomb and Yoerger's works (1999a; 1999b), the authors executed an experimental verification and comparison study with previous models, and proposed a model based thrust controller. In the two-state model, lift and drag were considered as sinusoidal functions, however, to increase model match with experimental results, Bachmayer et al. (2000) changed it to look-up table based non-sinusoidal functions, and presented a lift and drag parameter adaptation algorithm (Bachmayer and Whitcomb, 2003). Blanke et al. (2000) proposed a three-state model which also contains vehicle dynamics. Vehicle velocity effect was analyzed using non-dimensional propeller parameters, thrust coefficient and advance ratio. However, in the whole range of the advance ratio, the model does not match experimental results well.

In the former studies, there are three major restrictions. First, thruster dynamics are mostly modeled under the bollard pull condition, which means the effects of vehicle velocity or ambient flow velocity are not considered. However, while the thruster is operating, naturally, the underwater vehicle system is continuously moving or hovering against the current. In addition, the thrust force would be degraded by up to 30% of bollard output due to ambient flow velocity. Therefore, the bollard pull test results are only valid at the beginning of the operation, and the ambient flow velocity induced by vehicle movement or current must be taken into consideration. Moreover, non-parallel ambient flow effects have received less attention in previous works (Saunders and Nahon, 2002). These are dominant when an underwater vehicle changes its direction, or when an omni-directional underwater vehicle with non-parallel thrusters

like ODIN (Choi et al., 1995) is used. Non-parallel ambient flow effects could be modeled simply by multiplying the ambient flow by the cosine function, but experimental results have been inconsistent. Second, in the models including the ambient flow effect, the thrust equations are derived from approximations of empirical results without concern for physical and hydrodynamical analysis. This leads to a lack of consistency in the whole thrust force map, especially, when the directions of thrust force and ambient flow velocity are opposite. Third, most of the previous models contain axial flow velocity of the thruster, because the models are usually based on Bernoulli's equation and momentum conservation. However, measuring axial flow velocity is not feasible in real systems, so we cannot apply those equations directly to the controller. Hence, in Fossen and Blanke's work (2000), the authors used an observer and estimator for the axial flow velocity. And, Whitcomb and Yoerger (1999b) used the desired axial velocity as an actual axial flow velocity for the thrust controller. Those approaches, however, increase the complexity of controller.

To resolve the above restrictions, in this paper, we mainly focus on steady-state response of thrust force considering the effects of ambient flow and its incoming angle, and propose a new thruster model which has three outstanding features that distinguish it from other thruster models. First, we define the axial flow velocity as the linear combination of ambient flow velocity and propeller shaft velocity, which enables us to precisely fit the experimental results with theoretical ones. The definition of axial flow gives a physical relationship between the momentum equation and the non-dimensional representation, which has been widely used to express the relation between ambient flow velocity, propeller shaft velocity, and thrust force. Also, the modeling requires only measurable states, so it is practically feasible. Second, we divide the whole thrust force map into three states according to the advance ratio. The three states, equi-, anti-, and vague directional states, explain the discontinuities of the thrust coefficient in the non-dimensional plot. While the former approaches failed to consider anti- and vague directional states, the proposed model includes all of the flow states. Here, we define the value of border status between anti- and vague directional states as *Critical Advance Ratio (CAR)* where the patterns of streamline change sharply. The details will be given in Section 4.1. Third, based on the two above features, we develop the incoming angle effects to thrust force. Incoming angle means the angle between ambient flow and thruster, which is easily calculated from vehicle velocity. If the incoming angle is 0 degree, the thrust force coincides with the equi-directional state, or if the angle is 180 degree, the thrust force coincides with the vague or anti-directional state according to the advance ratio. It should be pointed out that the mid-range of incoming angle cannot be described by a simple trigonometric function of advance ratio. So we analyze the characteristics of incoming angle, and divide the whole angle region into the three states above. Also, for the border status among the states, *Critical Incoming Angle (CIA)* is defined.

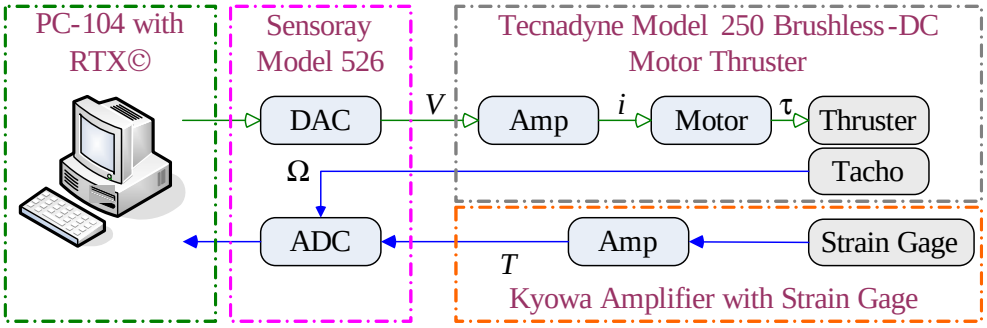

Fig. 1. Schematic diagram of experimental setup.

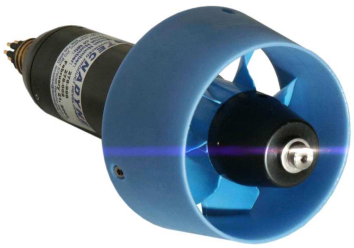

Fig. 2. Tecnadyne model 250 thruster.

This paper is organized as follow: Section 2 describes the experimental setup. In Section 3, the thruster modeling procedure will be explained and a new model for the thruster is derived. Section 4 addresses three fluid states with CAR and CIA, and explains the physical meanings. Then Section 5 describes the matching results of experiments with the proposed model simulation, and compares these results with conventional thrust models. Finally, concluding remarks will summarize the results.

2 Experimental setup

For model verification, we executed experiments using a commercial thruster. In this section, the experimental setup is briefly explained. Figure 1 shows the schematic diagram of experimental system composed of:

- an industrial PC running RTX© real-time extension,
- a Sensoray model 526 PC-104 data acquisition card,
- a Tecnadyne model 250 Brushless-DC motor thruster (Fig. 2), and
- a strain gage with Kyowa amplifier.

The thruster is composed of a 7cm diameter 7-blade Nylon propeller, and a 5.1cm length Kort nozzle. It has an internal velocity-loop controller operated

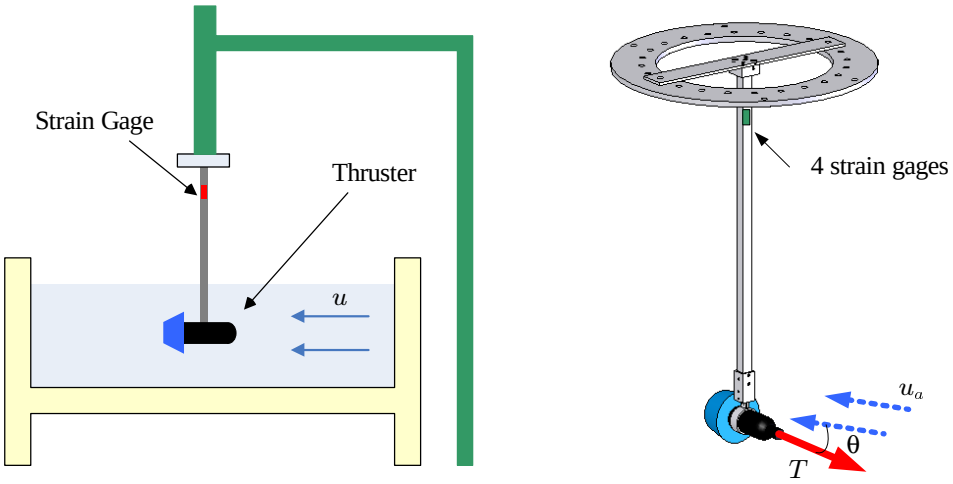

Fig. 3. Layout of experimental setup.

by an input voltage range of -5V to 5V, and a tachometer to give rotational velocity. The bollard output of the thruster is reported as 5.4kgf forward and 2.1kgf reverse.

The thruster was placed in a circulating water channel with a beam where the strain gage was attached. To simulate the vehicle velocity, the fluid velocity was varied from 0m/s to 1.2m/s. To verify incoming angle effects, the upper part of the structure was designed to change the orientation of thrust by 5 degree increments. The experimental setup is shown in Fig. 3. Four strain gages were attached to the beam, and the calibration was executed in air with known masses. The test results showed linear behavior according to mass variations.

The proposed model was verified by experiments with various forward fluid velocities in the circulating water channel. Strictly speaking, to consider precisely the effect of ambient flow velocity, we should experiment with a real vehicle and thruster in a long basin. However, in that case, too many uncertain parameters are involved, so we just did experiments for various forward fluid velocities instead of real vehicle velocities. Also, in this paper, we assume the forward fluid velocity is the same as ambient flow velocity and vehicle velocity. The nomenclature is defined in Table 1.

3 Thrust model with motor and fluid dynamic

The following section describes existing approaches for thruster modeling and explains ours. First, the motor dynamic model is introduced, and it is verified by propeller shaft velocity response. Next, the fluid model is described with the Bernoulli relation and linear momentum conservation. Finally, the physical

Table 1
Nomenclature

Name	Description
V_{in}	Voltage controlled input (V)
Ω	Propeller shaft velocity (rad/s)
T	Propeller thrust (N)
Q	Propeller shaft torque (Nm)
u_p	Axial fluid velocity at propeller (m/s)
u_a	Ambient axial fluid velocity (advance speed) (m/s)
u	Vehicle velocity (m/s)
K_T	Thrust coefficient (-)
J_0	Advance ratio (-)
J^*	Critical advance ratio (CAR) (-)
ρ	Density of water (kg/m^3)
m	Effective mass of water (kg)
D	Propeller disk diameter (m)
A_p	Propeller disk area (m^2)
t	Thrust deduction number (-)
w	Wake fraction number (-)

relationship between the fluid model and non-dimensional thrust coefficient is analyzed.

3.1 Motor model

In general, the thruster motor and propeller combination possess electro-mechanical dynamics with voltage-control mode as follows (Bachmayer et al., 2000):

$$\dot{\Omega} = k_t V_{in} - f(\Omega) - k_q Q, \tag{1}$$

where $f(\Omega)$ denotes the frictional effect, Q means shaft torque, and k_q is the shaft torque coefficient. However, in a real system, to measure the shaft torque is not easy, and the velocity control loop is assumed to compensate for shaft torque effect. Generally, a friction model in mechanical systems is dominated by coulomb and viscous friction. Hence, Eq. (1) can be rewritten as

$$\dot{\Omega} = k_t V_{in} - k_{f1}\Omega - k_{f0}\mathrm{sgn}(\Omega), \tag{2}$$

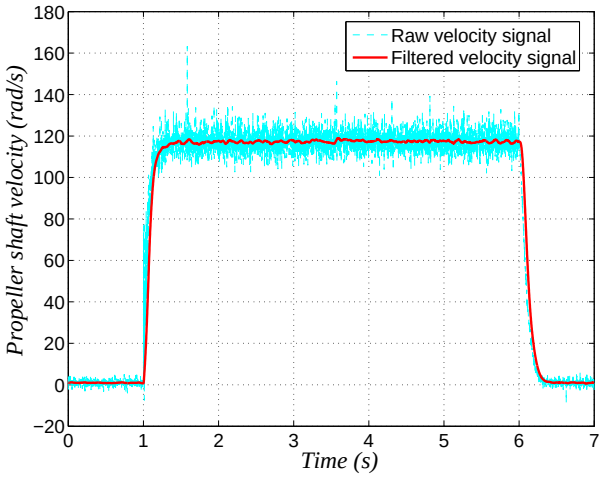

Fig. 4. Raw and filtered signal of propeller shaft velocity (3V input).

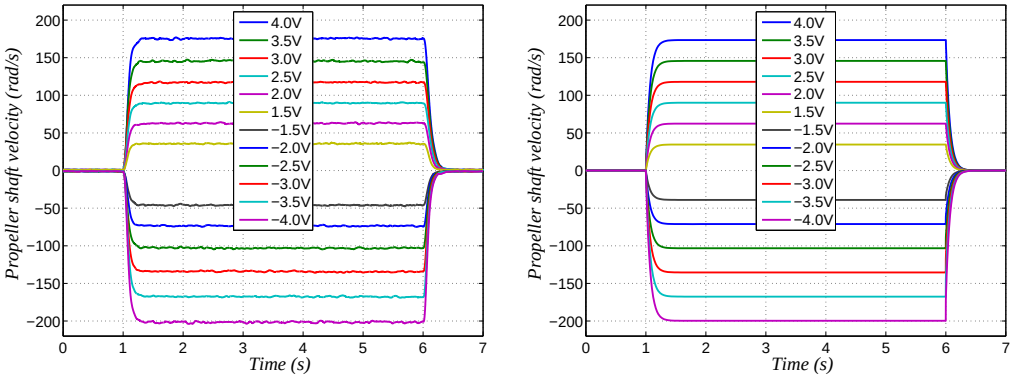

(a) (b)

Fig. 5. Propeller shaft velocity response: (a) experiment; and, (b) simulation.

where k_{f1} and k_{f0} are viscous and coulomb friction coefficients, respectively. Eq. (2) can be also expressed using a dead-zone model as below:

$$\dot{\Omega} = k_t \left(V_{in} - \frac{k_{f0}}{k_t} \mathrm{sgn}(\Omega) \right) - k_{f1}\Omega. \tag{3}$$

In our experimental setup, the propeller shaft velocity is acquired by the tachometer output. In contrast to the encoder signal, the tacho output is very noisy, so we cannot use it directly. In our experiments, to reduce noise, the Butterworth second order low pass filter was used to filter signal as shown in Fig. 4. Figure 5 shows the dynamic response of motor and propeller. Figure 5(a) and 5(b) are experimental and simulation results, which are almost identical. Figure 6 represents the propeller shaft velocity mapping along the input voltage. From this figure, the map has linear relationships with input voltage, a dead-band around zero, and saturation regions.

In the experiments, the propeller shaft velocity did not vary much regardless

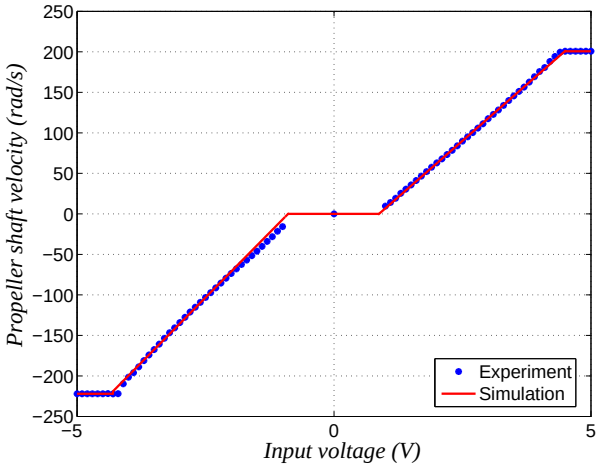

Fig. 6. Propeller shaft velocity map.

of ambient fluid velocity, which means the velocity control loop compensates for the shaft torque effects successfully as per our assumption. However, this ambient velocity affects thrust force greatly, as will be shown in the following section.

3.2 Fluid model of the propeller

Healey et al. (1995) developed a two-state thruster model as below:

$$\dot{u}_p = N_T T - N_u(u_p - u)|u_p - u|, \tag{4}$$
$$T = T(\Omega, u_p), \tag{5}$$

where N_T and N_u are constant coefficients. And, to obtain the four-quadrant thruster characteristics, they introduced sinusoidal lift and drag coefficients.

Fossen and Blanke (2000) proposed a three-state model with vehicle dynamics.

$$\dot{u}_p = N_T T - N_{u0} u_p - N_u(u_p - u_a)|u_p|, \tag{6}$$
$$m_f \dot{u} + d_1 u + d_2 u|u| = (1-t)T, \tag{7}$$
$$u_a = (1-w)u, \tag{8}$$
$$T = T(\Omega, u_p), \tag{9}$$

where N_T, N_u, and N_{u0} are constant coefficients, and, m_f is vehicle mass, and d_1 and d_2 are drag coefficients.

The above two approaches mainly focus on the dynamic response with axial flow velocity rather than the ambient flow velocity. However, initially, they assumed quasi-stationary flow and used the Bernoulli relations which are valid

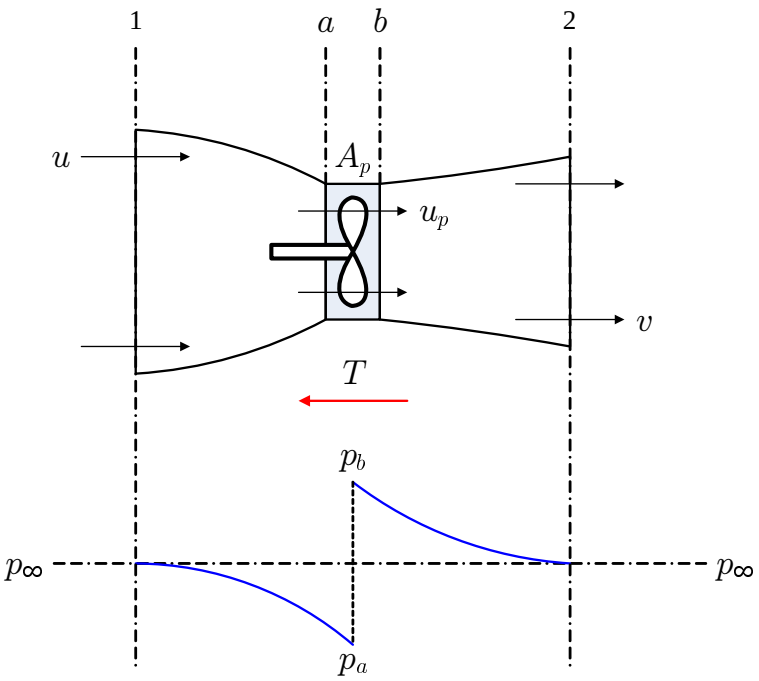

Fig. 7. Propeller race contraction; velocity and pressure changes.

only for fully developed flow, so the dynamic relations are less meaningful. And, to construct thrust controller, they tried to find a solution to estimate the axial flow velocity, because the axial flow is a non-measurable state. In contrast to the previous methods, we only consider the steady-state model and define axial flow as measurable states as will be shown in the following.

The propeller is represented by an actuator disk which creates across the propeller plane a pressure discontinuity of area A_p and axial flow velocity u_p. The pressure drops to p_a just before the disk and rises to p_b just after and returns to free-stream pressure, p_∞, in the far wake. To hold the propeller rigid when it is extracting energy from the fluid, there must be a leftward thrust force T on its support, as shown in Fig. 7.

If we use the control-volume-horizontal-momentum relation between sections 1 and 2,

$$T = \dot{m}(v - u). \tag{10}$$

A similar relation for a control volume just before and after the disk gives

$$T = A_p(p_b - p_a). \tag{11}$$

Equating these two yields the propeller force

$$T = A_p(p_b - p_a) = \dot{m}(v - u). \tag{12}$$

Assuming ideal flow, the pressures can be found by applying the incompressible

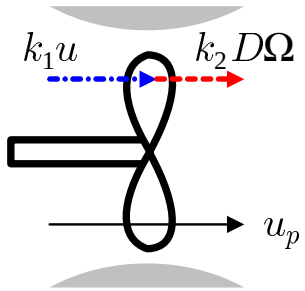

Fig. 8. Proposed axial flow model.

Bernoulli relation up to the disk

$$\begin{aligned} &\text{From 1 to a:} \qquad p_\infty + \tfrac{1}{2}\rho u^2 = p_a + \tfrac{1}{2}\rho u_p^2, \\ &\text{From b to 2:} \qquad p_\infty + \tfrac{1}{2}\rho v^2 = p_b + \tfrac{1}{2}\rho u_p^2. \end{aligned} \tag{13}$$

Subtracting these and noting that $\dot{m} = \rho A_p u_p$ through the propeller, we can substitute for $p_b - p_a$ in Eq. (12) to obtain

$$p_b - p_a = \frac{1}{2}\rho(v^2 - u^2) = \rho u_p (v - u), \tag{14}$$

or

$$u_p = \frac{1}{2}(v + u) \Rightarrow v = 2u_p - u. \tag{15}$$

Finally, the thrust force by the disk can be written in terms of u_p and u by combining Eqs. (12) and (15) as follows:

$$T = 2\rho A_p u_p (u_p - u). \tag{16}$$

Up to this point, the procedures are the same as the previous approaches. Now, we define the axial flow velocity as

$$u_p \triangleq k_1 u + k_2 D\Omega, \tag{17}$$

where k_1 and k_2 are constant. The schematic diagram of the axial flow relation is shown in Fig. 8. For quasi-stationary flow, the axial flow only depends on ambient flow and propeller rotational motion. More complex combinations of ambient flow and propeller velocity are possible, but this linear combination is adequate as will be shown later. This somewhat simplified definition gives lots of advantages and physical meanings.

Finally, substituting Eq. (17) to Eq. (16), the proposed thrust model can be derived as follows:

$$\begin{aligned} T &= 2\rho A_p (k_1 u + k_2 D\Omega)(k_1 u + k_2 D\Omega - u), \\ &= 2\rho A_p (k_1' u^2 + k_2' u D\Omega + k_3' D^2 \Omega^2). \end{aligned} \tag{18}$$

This model will be used in the following non-dimensional analysis.

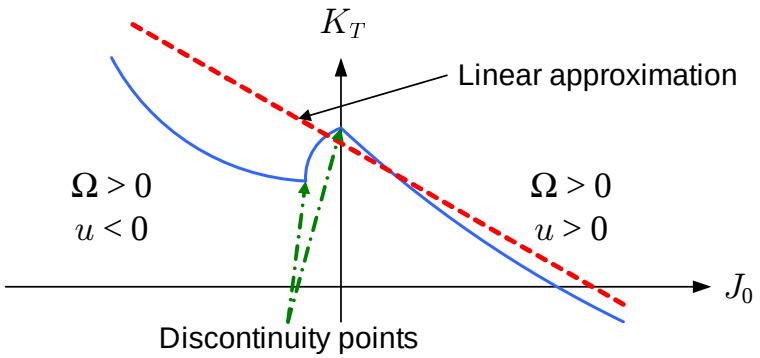

Fig. 9. Thrust coefficient as a function of advance ratio and its linear approximation.

3.3 Non-dimensional analysis

The non-dimensional representation for thrust coefficient has been widely used to express the relation between thrust force, propeller shaft velocity and ambient flow velocity as below:

$$K_T(J_0) = \frac{T}{\rho D \Omega |\Omega|}, \tag{19}$$

where

$$J_0 = \frac{u}{D\Omega} \tag{20}$$

is the advance ratio. Figure 9 shows a typical non-dimensional plot found in various references (Manen and Ossanen, 1988; Blanke et al., 2000). In former studies, the non-dimensional relation is only given as an empirical look-up table or simple linear relationship for the whole non-dimensional map as (Fossen and Blanke, 2000)

$$K_T(J_0) = a_1 J_0 + a_2. \tag{21}$$

However, as shown in Fig. 9, Eq. (21) cannot accurately describe the characteristics of the thrust coefficient, especially when $J_0 < 0$, and, rather than a linear equation, the thrust coefficient seems to be close to a quadratic equation except for the discontinuity points. Even more, Eq. (21) has no physical relationship with thrust force, but is just a linear approximation from the figure.

The proposed axial flow assumption would give a solution for this. The non-dimensionalization of Eq. (18) is expressed as

$$\frac{T}{\rho D^4 \Omega^2} = \frac{\pi}{2}\left[k_1' \left(\frac{u}{D\Omega}\right)^2 + k_2' \frac{u}{D\Omega} + k_3'\right]. \tag{22}$$

And, the quadratic thrust coefficient relation is obtained as following:

$$K_T(J_0) = \frac{\pi}{2}\left[k_1' J_0^2 + k_2' J_0 + k_3'\right]. \tag{23}$$

Hence, contrary to other models, the axial flow definition of Eq. (17) gives an appropriate relationship between the thrust force equation and non-dimensional plot since the derivation was done by physical laws. Also, Eq. (23) can explain the characteristics of the quadratic equation of the thrust coefficient. From this phenomenon, we can perceive that the axial flow definition in Eq. (17) is reasonable. The coefficients of quadratic equations could be changed depending on hardware characteristics. However, there is still a question of the discontinuities of thrust coefficient in Fig. 9 which has not been answered yet by existing models. This problem will be addressed in the following section.

4 Thrust force with ambient flow model

If ambient flow varies, thrust force changes even with the same propeller shaft velocity, which means that the ambient flow disturbs the flow state under the bollard pull condition. Flow state is determined by a complex relation between propeller shaft velocity, ambient flow velocity and its incoming angle. This will be shown in the following subsections.

4.1 Flow state classification using CAR

In this subsection, we define three different flow states according to the value of advance ratio and the condition of axial flow. To distinguish them, we introduce *Critical Advance Ratio (CAR)*, J^*.

The three states are as below:

- Equi-directional state

$$J_0 > 0, \tag{24}$$
$$u_p = k_1 u + k_2 D\Omega > 0. \tag{25}$$

- Anti-directional state

$$J^* < J_0 < 0, \tag{26}$$
$$u_p = k_1 u + k_2 D\Omega > 0. \tag{27}$$

- Vague directional state

$$J^* > J_0, \tag{28}$$
$$u_p = k_1 u + k_2 D\Omega < 0. \tag{29}$$

Figure 10 shows the flow states schematically.

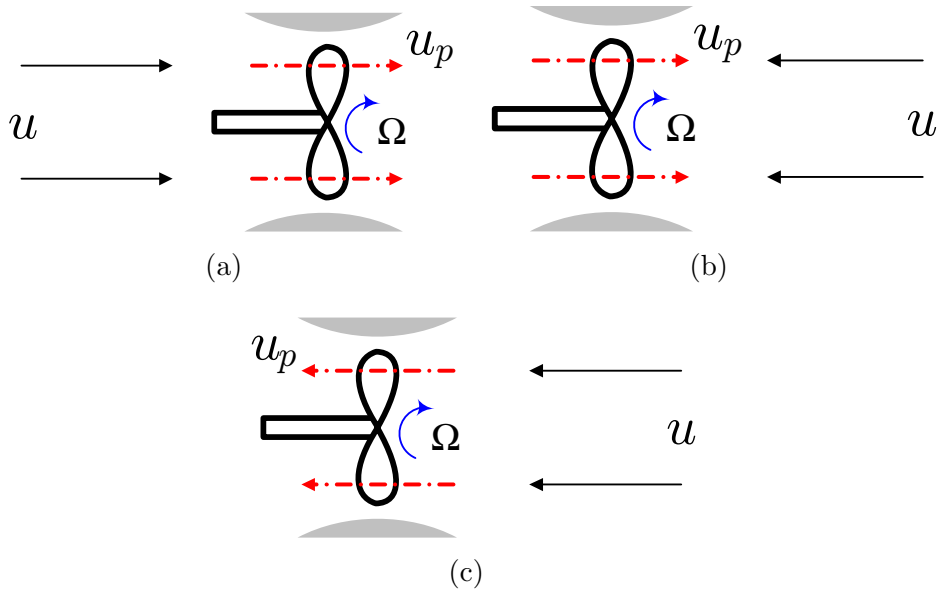

Fig. 10. Three flow states: (a) equi-directional state; (b) anti-directional state; and, (c) vague directional state.

Equi-directional state : The equi-directional state occurs when the ambient flow direction and axial flow direction coincide. In this state, if the ambient flow velocity increases, the pressure difference decreases. Hence the thrust force reduces, and the streamline evolves as a general form. (Fig. 10(a))

Anti-directional state : The anti-directional state happens when the ambient flow and axial flow direction are opposite. However, the axial flow can thrust out the ambient flow, hence the streamline can be built as sink and source. The Bernoulli equation can be applied and the thrust equation is still valid but the coefficients are different from those of the equi-directional state. Also, the thrust force rises as the ambient flow velocity increases, because the pressure difference increases. (Fig. 10(b))

Vague directional state : In the vague directional state, the axial flow cannot be well defined. The axial flow velocity cannot thrust out the ambient flow, hence the direction of axial flow is not obvious. This ambiguous motion disturbs the flow, so the thrust force reduces. In this case, we cannot guess the form of the streamline, so the thrust relation cannot be applied. However, the experimental results show the proposed thrust relation is still valid in this state. (Fig. 10(c))

Former studies did not consider the anti- and vague directional states, however they can be observed frequently when a vehicle tries to stop or reverse direction. The CAR divides between the anti- and vague directional states as shown in Fig. 11. It would be one of the important characteristics of a thruster. At this CAR point, the ambient flow and propeller rotational motion are kept

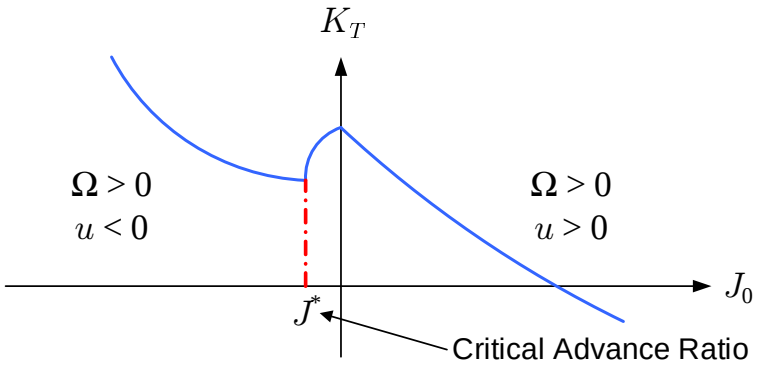

Fig. 11. Thrust coefficient as a function of advance ratio and Critical Advance Ratio (CAR).

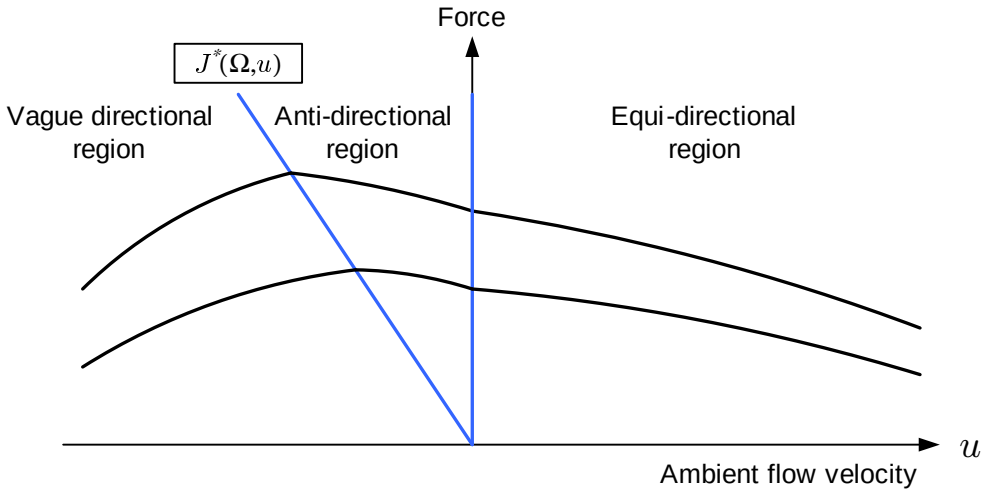

Fig. 12. Thrust force as a function of ambient flow velocity.

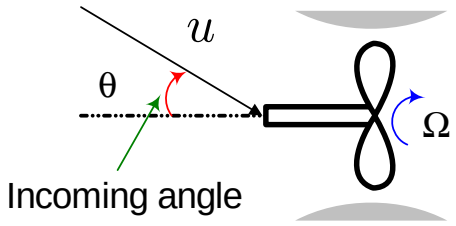

Fig. 13. Incoming angle of ambient flow.

in equilibrium. Hence, to increase the efficiency of the thruster in the reverse thrust mode, an advance ratio value larger than the CAR is preferable, as shown in Fig. 12.

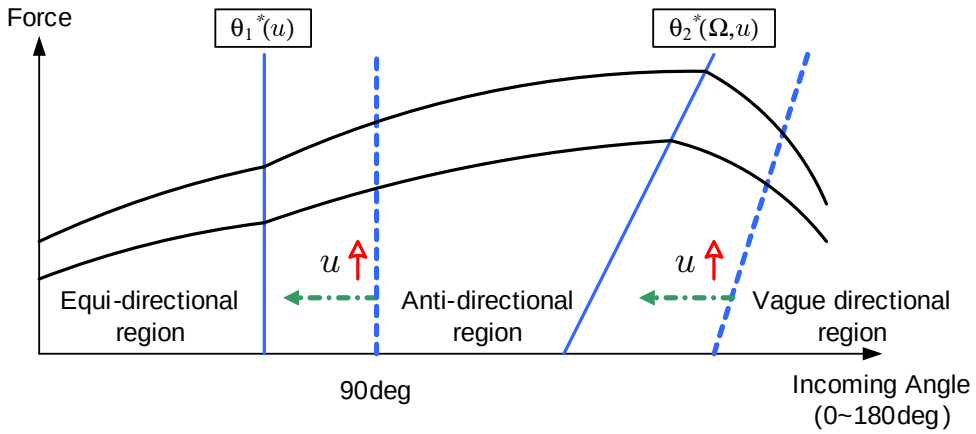

Fig. 14. Thrust force as a function of incoming angle.

4.2 Effects of incoming angle on thrust force

In this subsection, the incoming angle effect on thrust force is analyzed. Figure 13 shows the definition of incoming angle. Naturally, if the angle between ambient flow and thrust force is non-parallel, the thrust force varies with the incoming angle. Basically, by multiplying ambient flow velocity by the cosine of the incoming angle, the thrust force can be derived from Eq. (23). In that case, however, the calculated thrust force will not coincide with experimental results except at 0 and 180 degrees, which shows that the incoming angle and ambient flow velocity have another relationship. Hence, we develop the relationship based on experiments, and Fig. 14 shows the result.

In Fig. 14, the whole range of angles is also divided into three state regions as denoted in the previous subsection. And, we define the borders of the regions as *Critical Incoming Angles (CIA)* which have the following mathematical relationship.

$$\theta_1^*(u) = \pi/2 - a_1 u, \tag{30}$$
$$\theta_2^*(\Omega, u) = a_2 u(\Omega - b_2) + c_2 + \theta_1^*, \tag{31}$$

where a_1, a_2, b_2, and c_2 are all positive constants. And, $\theta_1^*(u)$ and $\theta_2^*(\Omega, u)$ are the first and second CIA, respectively. Theoretical reasons have not been developed to explain the CIA equations, but empirical results give a physical insight and the above equations can be correlated to experiments. The equi-directional region and anti-directional region are differentiated with the first CIA. The first CIA only depends on the ambient flow velocity. At the first CIA, the thrust coefficient is the same as the thrust coefficient with no ambient flow velocity. The second CIA separates the anti-directional region and the vague directional region. The second CIA depends not only on ambient flow angle but also on propeller shaft velocity. From Eqs. (30) and (31), the three regions

shift to the left as the ambient flow velocity increases.

Now, we derive the incoming angle effect on the thrust force as following:

$$K_T^a = K_T^0 + f_a(J_0, \theta), \tag{32}$$
$$T = K_T^a \cdot \rho D^4 \Omega |\Omega|, \tag{33}$$

where $K_T^0 = K_T(J_0 = 0)$, and

$$f_a = \begin{cases} (K_T^0 - K_T^+)\left[\sin\left(\frac{\theta}{\theta_1^*}\frac{\pi}{2}\right) - 1\right], & (0 \le \theta \le \theta_1^*) \\ K_a J_0 \sin\left(\frac{\theta-\theta_1^*}{\pi-\theta_1^*}\frac{\pi}{2}\right), & (\theta_1^* < \theta \le \theta_2^*) \\ \left[K_a J_0 \sin\left(\frac{\theta_2^*-\theta_1^*}{\pi-\theta_1^*}\frac{\pi}{2}\right) - (K_T^- - K_T^0)\right]\cos\left(\frac{\theta-\theta_2^*}{\pi-\theta_2^*}\frac{\pi}{2}\right) + (K_T^- - K_T^0). & (\theta_2^* < \theta \le \pi) \end{cases} \tag{34}$$

In Eq. (34), K_a is a constant which has to be acquired by experiments. $K_T^+ = K_T(J_0)$ and $K_T^- = K_T(-J_0)$. Eq. (32) coincides with Eq. (23) at 0 and 180 degree. Hence Eq. (32) contains all of the effects of ambient flow and implies that the total thrust force is composed of thrust force with bollard pull condition, K_T^0, and additional force induced by ambient flow velocity and its incoming angle, $f_a(J_0, \theta)$.

5 Experimental results

To verify the proposed model, firstly, we operated the thruster under various ambient flow velocities: ±1.2m/s, ±1.0m/s, ±0.8m/s, ±0.6m/s, ±0.4m/s, and 0m/s with a zero degree incoming angle. Then, for 0.4m/s, 0.6m/s and 0.8m/s ambient flow velocities, the thruster was tilted at 5 degree increments from 0 to 180 degree to change incoming angle. For simplicity, we only consider cases where $\Omega > 0$.

Figure 15 shows the experimental thrust coefficient plot. As shown in the figure, the thrust coefficient is divided into three parts. The difference between Figs. 11 and 15 comes from hardware characteristics, for example, shape of duct, pitch ratio, etc. Hence the coefficients of quadratic equations should be identified from experimental results.

In Fig. 16, the experimental thrust forces are compared with simulation results of the proposed model with an input voltage range from 1.5V to 4.5V. Both results are very similar except at some localized points. The deviation could be caused by the thruster not being located in sufficiently deep water due to the restriction of the experimental environment. Thus, the anti- and vague directional response could have been disturbed by spouting water.

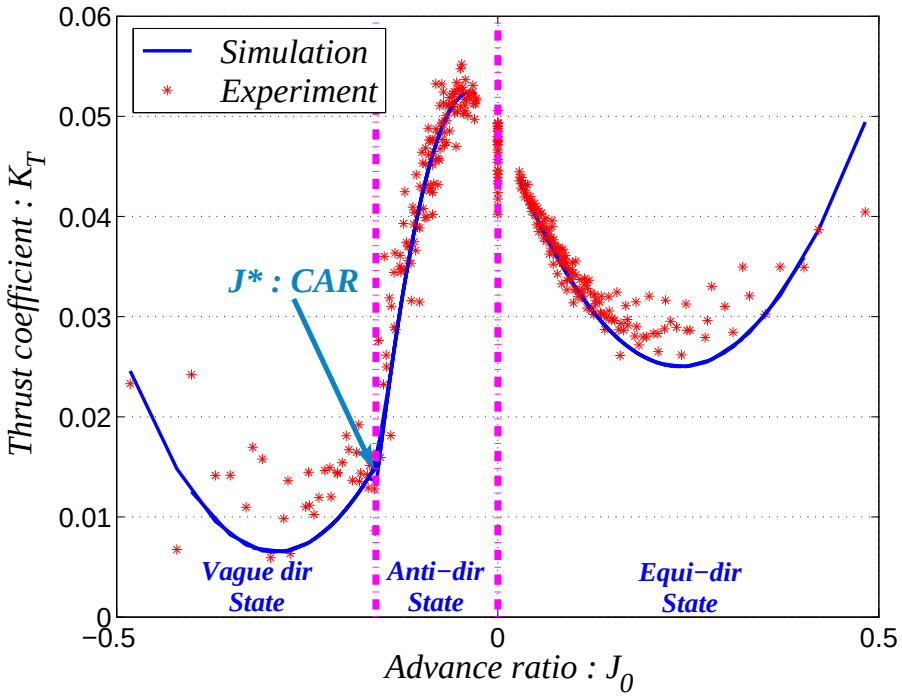

Fig. 15. Experimental thrust coefficient as a function of advance ratio.

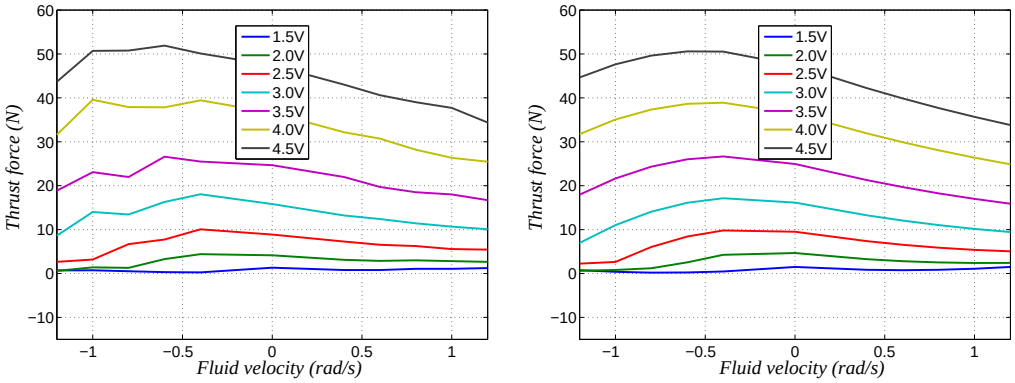

Fig. 16. Comparison results of experiment and simulation by the proposed model : (a) thrust force - experiment; and, (b) thrust force - simulation.

As the ambient flow velocity decreases, the thrust force initially increases until the CAR and decreases after crossing the CAR. Figure 17 shows the result of the propeller shaft velocity versus the thruster force under various ambient flow velocities. The results indicate that the proposed thruster model provides high accuracy in the whole range of thrust force map. As shown in Figs. 17(a), 17(b), and 17(c), the thrust forces are modeled using two quadratic equations due to the CAR.

To highlight the performance of the proposed model, we compare the results with those of the conventional model described by Eq. (21). The comparison

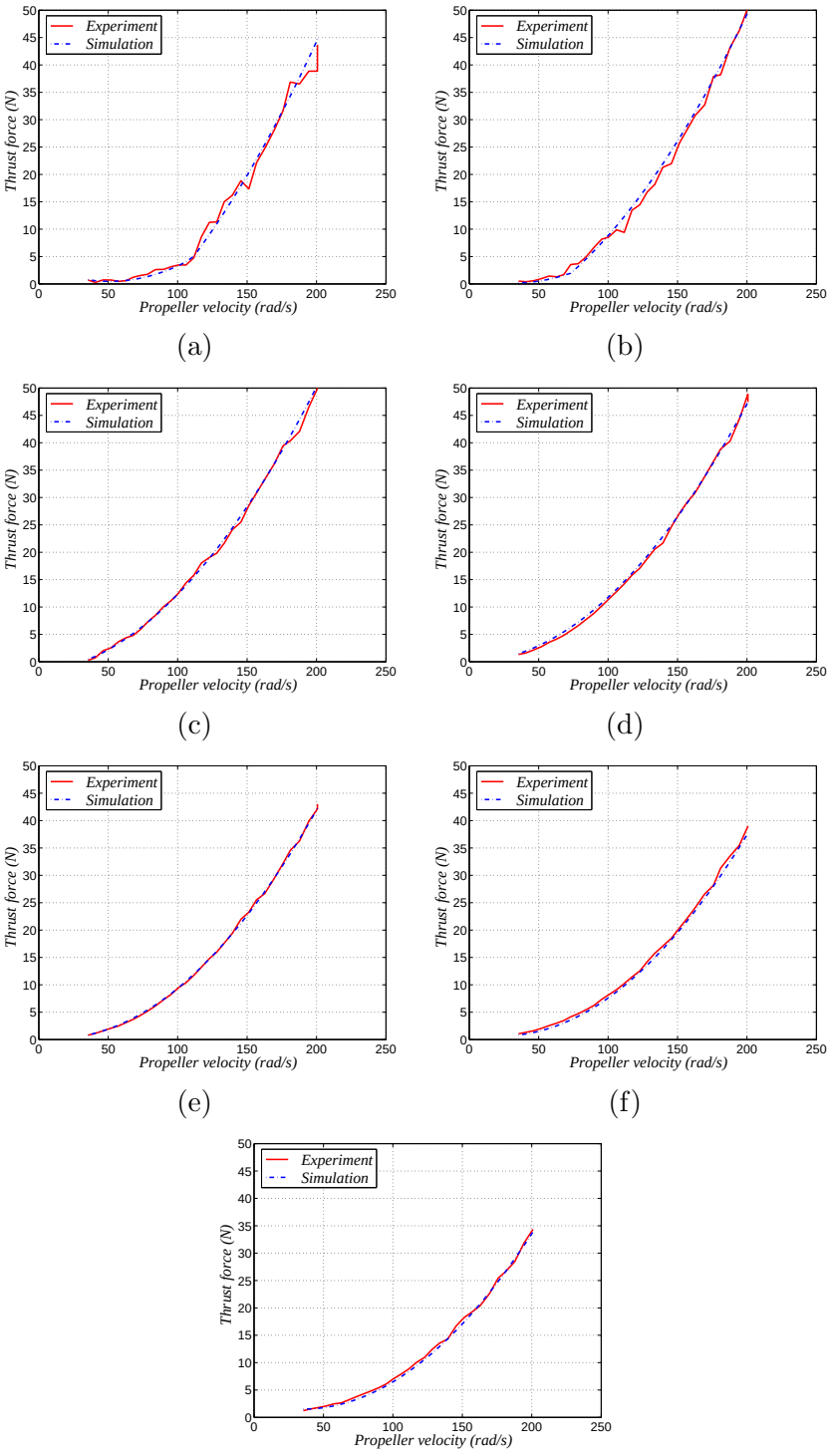

Fig. 17. Comparison results of experiment and simulation: (a) -1.2m/s ambient flow velocity; (b) -0.8m/s ambient flow velocity; (c) -0.4m/s ambient flow velocity; (d) 0.0m/s ambient flow velocity; (e) 0.4m/s ambient flow velocity; (f) 0.8m/s ambient flow velocity; and, (g) 1.2m/s ambient flow velocity.

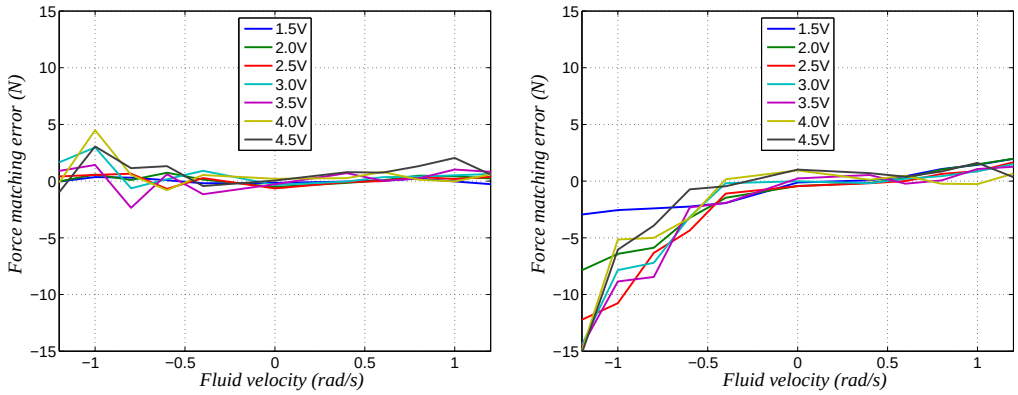

(a) (b)

Fig. 18. Thrust force matching error : (a) by the proposed model; and, (b) by the conventional model.

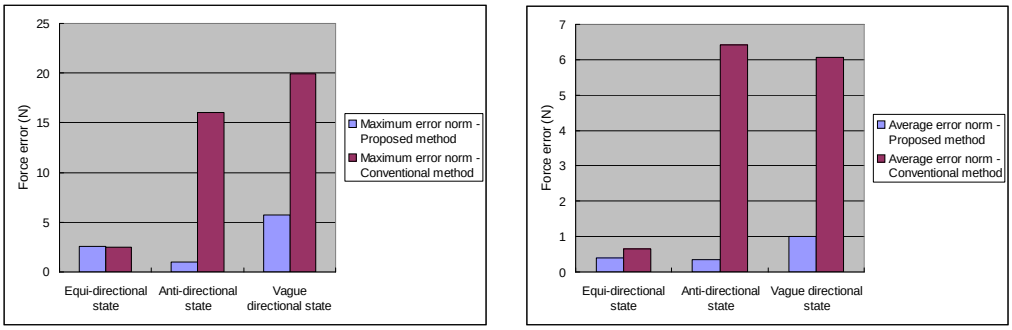

(a) (b)

Fig. 19. Thrust force matching error comparison : (a) maximum error; and, (b) average error.

results are shown in Figs. 18 and 19. These figures show that our results are significantly better than the conventional model in the anti- and vague directional regions.

Figure 20 shows the matching results between experiment and simulation with the multiplication of cosine function to ambient flow. As shown in figure, the matching errors increase as the ambient flow velocity goes fast. Hence, this model makes the control performance of underwater vehicles to be poor.

Figures 21(a), 21(c) and 21(e) show the thrust force comparison between experiment and simulation as a function of incoming angle. The errors of matching, as shown in Figs. 21(b), 21(d) and 21(f), are mostly within $\pm$2N. Note that the maximum force of the thrust is up to 50N.

From the matching results with ambient flow velocities and incoming angles, we can say that our initial definition of axial flow is valid, and the proposed model shows good agreement with experimental results under various ambient flow velocities and incoming angles.

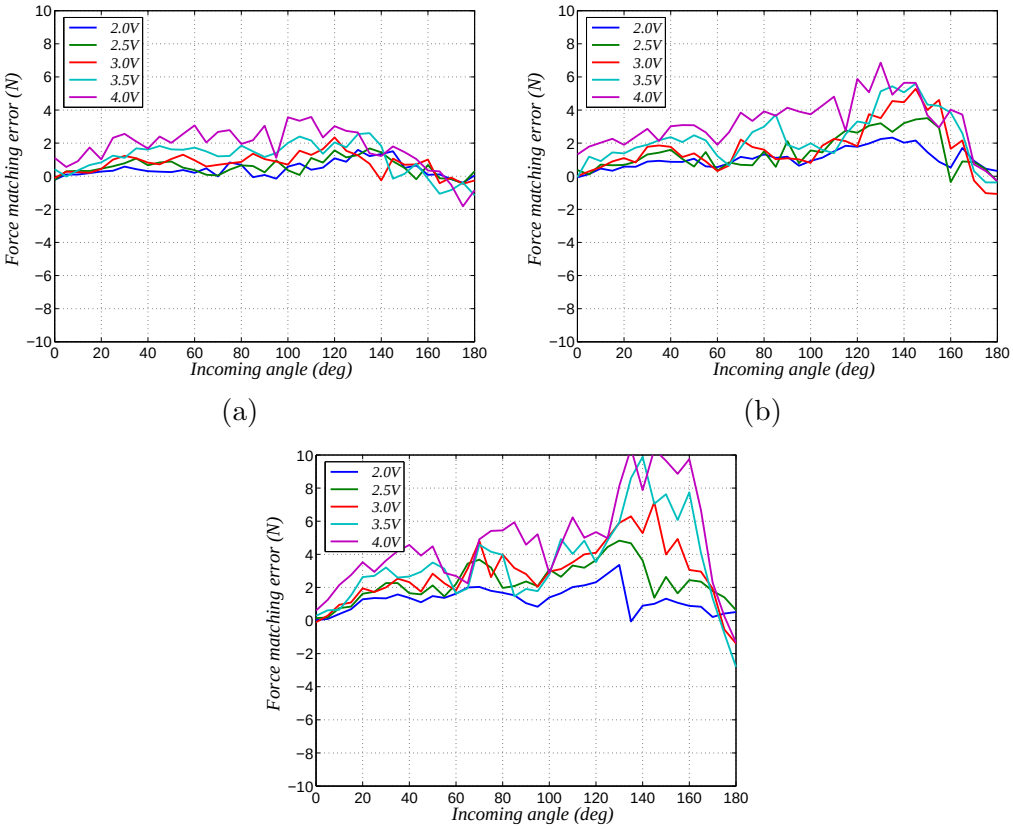

Fig. 20. Comparison results with the multiplication of cosine function to ambient flow : (b) matching error with 0.4m/s ambient flow velocity; (d) matching error with 0.6m/s ambient flow velocity; and, (f) matching error with 0.8m/s ambient flow velocity.

6 Conclusion

In this paper, we proposed a new model of thrust force. First, we define the axial flow as a linear combination of the ambient flow and propeller shaft velocity which are both measurable. In contrast to the previous models, the proposed model does not use the axial flow velocity which cannot be measured in real systems, but only uses measurable states, which shows the practical applicability of the proposed model. The quadratic thrust coefficient relation derived using the definition of the axial flow shows good matching with experimental results.

Next, three states, the equi-, anti-, and vague directional states, are defined according to advance ratio and axial flow state. The discontinuities of the thrust coefficient in the non-dimensional plot can be explained by those states. Although they have not been treated previous to this study, the anti- and vague directional states occur frequently when a vehicle stops or reverses direction.

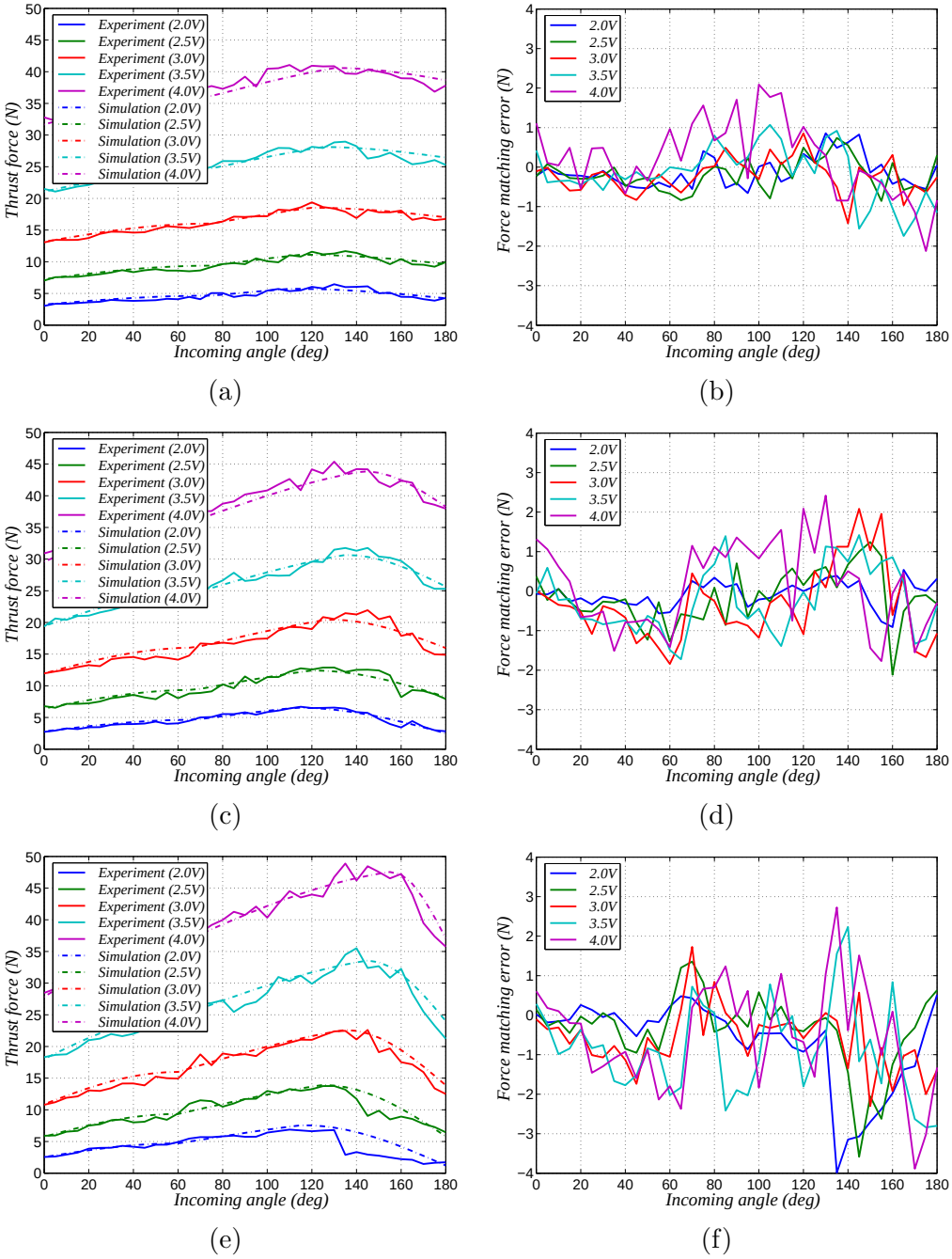

Fig. 21. Comparison results of experiment and simulation with incoming angle: (a) 0.4m/s ambient flow velocity; (b) matching error with 0.4m/s ambient flow velocity; (c) 0.6m/s ambient flow velocity; (d) matching error with 0.6m/s ambient flow velocity; (e) 0.8m/s ambient flow velocity; and, (f) matching error with 0.8m/s ambient flow velocity.

The anti- and vague directional states are classified by CAR (Critical Advance Ratio), which can be used to tune the efficiency of the thruster.

Finally, the incoming angle effects to the thrust force, which are dominant

in turning motions or for omni-directional underwater vehicles, are analyzed and CIA (Critical Incoming Angle) was used to define equi-, anti-, and vague directional regions.

The matching results between simulation with experimental results show excellent correlation with only $\pm$2N error in the entire space of thrust force under various ambient flow velocities and incoming angles. The results are also compared with conventional thrust models, and the matching performance with the proposed model is several times better than those of conventional linear ones.

Acknowledgement

The authors would like to thank J. Han who designed and built the thrust experimental environment and helped the experiments. They with to thank him for his generous contributions.

This research was supported in part by the International Cooperation Research Program("Development of Intelligent Underwater Vehicle/Manipulator and Its Control Architecture", M6-0302-00-0009-03-A01-00-004-00) of the Ministry of Science & Technology, Korea, and supported in part by the Ministry of Education and Human Resources Development (MOE) and the Ministry of Commerce, Industry & Energy (MOCIE) through the fostering project of the Industrial-Academic Cooperation Centered University.

References

Bachmayer, R., Whitcomb, L. L., Sep. 2003. Adaptive parameter identification of an accurate nonlinear dynamical model for marine thrusters. J. of Dynamic Sys., Meas., and Control 125 (3), 491–494.

Bachmayer, R., Whitcomb, L. L., Grosenbaugh, M. A., Jan. 2000. An accurate four-quadrant nonlinear dynamical model for marine thrusters: Theory and experimental validation. IEEE J. Oceanic Eng. 25 (1), 146–159.

Blanke, M., Lindegaard, K.-P., Fossen, T. I., 2000. Dynamic model for thrust generation of marine propellers. In: IFAC Conf. Maneuvering and Control of Marine Craft (MCMC'2000). pp. 23–25.

Choi, S. K., Yuh, J., Takashige, G. Y., Mar. 1995. Development of the omnidirectional intelligent navigator. IEEE Robotics and Automation Magazine 2 (1), 44–53.

Fossen, T. I., Blanke, M., Apr. 2000. Nonlinear output feedback control of underwater vehicle propellers using feedback form estimated axial flow velocity. IEEE J. Oceanic Eng. 25 (2), 241–255.

Healey, A. J., Rock, S. M., Cody, S., Miles, D., Brown, J. P., Oct. 1995. Toward an improved understanding of thruster dynamics for underwater vehicles. IEEE J. Oceanic Eng. 20 (4), 354–361.

Manen, J. D. V., Ossanen, P. V., 1988. Principles of Naval Architecture, Second Revision, Volume II: Resistance, Propulsion, and Vibration. Jersey City, NJ: Soc. of Naval Architects and Marine Engineers.

Newman, J. N., 1977. Marine Hydrodynamics. MIT Press, Cambridge, MA.

Saunders, A., Nahon, M., 2002. The effect of forward vehicle velocity on through-body AUV tunnel thruster performance. In: IEEE/MTS OCEANS '02. pp. 250–259.

Whitcomb, L. L., Yoerger, D. R., Oct. 1999a. Development, comparison, and preliminary experimental validation of nonlinear dynamic thruster models. IEEE J. Oceanic Eng. 24 (4), 481–494.

Whitcomb, L. L., Yoerger, D. R., Oct. 1999b. Preliminary experiments in model-based thruster control for underwater vehicle positioning. IEEE J. Oceanic Eng. 24 (4), 495–506.

Yoerger, D. R., Cooke, J. G., Slotine, J.-J. E., Jul. 1990. The influence of thruster dynamics on underwater vehicle behavior and their incorporation into control system design. IEEE J. Oceanic Eng. 15 (3), 167–178.